



The phase change problem in materials with internal heat generation in a cylinder

Lyudmyla L. Barannyk^{a,*}, John C. Crepeau^b, Patrick Paulus^b, Alexey Yu. Sakhnov^c, Sidney D.V. Williams^d

^a Department of Mathematics and Statistical Science, University of Idaho, 875 Perimeter Drive MS 1103, Moscow 83843, ID, USA

^b Department of Mechanical Engineering, University of Idaho, 875 Perimeter Drive MS 0902, Moscow 83843, ID, USA

^c Kutateladze Institute of Thermophysics SB RAS, 1 Lavrentyev Ave., Novosibirsk 630090, Russia

^d Department of Physics, University of California San Diego, 9289 S Scholars Dr., La Jolla 92093, CA, USA

ARTICLE INFO

Keywords:

Solid-liquid phase change
Stefan problem
Sharp interface
Melting and solidification
Overheated zone
Mushy zone
Separation of variables
Method of catching of the front into a space grid node
Enthalpy-porosity method

ABSTRACT

We analyze the evolution of the solid-liquid front during melting and solidification in materials with constant internal heat generation, under prescribed temperature and heat flux conditions at the boundary of an infinite cylinder. We employ a sharp interface approach and assume that the motion of the front is slow relative to the temperature changes in both phases of the material. We derive infinite series solutions for the temperature in each phase and a nonlinear first-order differential equation for the evolution of the interface. Additionally, we solve the problem using the catching of the front into a node method and the Ansys Fluent enthalpy-porosity method. The latter incorporates a mushy zone that is a mixed solid-liquid transition zone. All three methods provide consistent results, especially when the mushy zone is taken into account. The series and front catching solutions develop a finite time overheated zone during melting, whereas the enthalpy solutions do not exhibit this phenomenon. We show that the evolution of the overheated and mushy zones is very similar in shape and time for both boundary conditions.

1. Introduction

The classical solid-liquid phase change problem has been investigated for almost two centuries, beginning with the work by Lamé and Clapeyron [1], and later independently by Stefan [2], whose name became synonymous with this class of problems Rubenstein [3]. Stefan problems continue to be an active area of research today Alexiades and Solomon [4]; Lock [5]; Salva and Tarzia [6]. While the classical problem has been well analyzed, a subset of the problem, namely phase change driven by internal heat generation, has received much less attention. Various techniques have been employed to study phase change driven by internal heat generation including quasi-static models Crepeau and Siahpush [7], perturbation analysis Yu, Fan, Hu and Cen [8], lumped parameter techniques An and Su [9], and finite element Legendre wavelet Galerkin method Jitendra [10] among others.

Applications of phase change processes with internal heat generation include geological heat transfer Weinstein [11]; Furlong and Chapman [12], energy storage Rao, Wang and Zhang [13]; Ye and Arici [14],

nano-enhanced phase change materials Bechiri and Mansouri [15] as well as nuclear safety analysis Barzegari, Aghaie and Zolfaghari [16]. Chen et al. [17] employed a simple transient conduction model to determine the onset of melting in a nuclear fuel pin. El-Genk and Cronenberg [18] analyzed the effects of internal heat generation on transient freezing in a reactor shield plug using a successive approximation technique. Cheung et al. [19] examined melting and freezing in a heat generating slab between two semi-infinite walls. Chan et al. [20] modeled phase change in semi-transparent materials induced by radiation heat transfer. Chan and Hsu [21] used the enthalpy method to study the formation of the mushy zone in problems with internal heat generation. Le Tellier, et al. [22] employed three different techniques to study the Stefan problem and included the effects of convection in the liquid phase to study the boundary heat flux closure relations. Tang et al. [23] conducted a numerical study on melting processes in a nuclear fuel rod using the half-boundary method applied to an enthalpy formulation. Dubey and Sharma [24] coupled the melting problem with the multi-phase flow of nuclear fuel in a fast reactor fuel rod. An et al. [25] utilized finite difference techniques to study the melting processes in a

* Corresponding author.

E-mail addresses: barannyk@uidaho.edu (L.L. Barannyk), crepeau@uidaho.edu (J.C. Crepeau), patrickpaulus@gmail.com (P. Paulus), aleksei_sakhnov@mail.ru (A.Yu. Sakhnov), siw038@ucsd.edu (S.D.V. Williams).

Nomenclature

$A_n, B_n, \tilde{A}_n, \tilde{B}_n$	Fourier-Bessel series coefficients
c_p	specific heat, [J/(kg·K)]
Δh_f	latent heat of fusion, [J/kg]
J_0, Y_0	Bessel functions of the first and second kind of order 0, respectively
J_1, Y_1	Bessel functions of the first and second kind of order 1, respectively
k	thermal conductivity, [W/(m·K)]
\dot{q}	internal heat generation, [W/m ³]
\dot{Q}	nondimensional heat generation
q''_0	surface heat flux, [W/m ²]
r	distance in the radial direction, [m]
r_0	radius of the cylinder, [m]
s	distance to the phase change front from the centerline, [m]
St	Stefan number

t	time, [s]
T	temperature, [K]
T_0	temperature along the surface of the cylinder, [K]
T_m	phase change temperature, [K]
z_{0n}	zeros of the Bessel function of 0th order
α	thermal diffusivity, [m ² /s]
ϕ, Φ	initial temperature profiles, [K]
η	nondimensional distance
$\lambda, \tilde{\lambda}, \hat{\lambda}, \tilde{\hat{\lambda}}$	eigenvalues
θ	nondimensional temperature
ρ	density, [kg/m ³]
τ	nondimensional time
ζ	nondimensional distance to the phase change front from the centerline
liq	liquid
sol	solid

nuclear fuel rod. Alsulami et al. [26] conducted a quasi-steady analysis and used convective cooling of phase change materials subject to internal heat generation to show the role of the Biot number on the transient evolution of the solidification front. Wang et al. [27] applied a three phase Eulerian multiphase flow method to model a phase change process of melting and solidification of frost by including a source term, showing higher prediction accuracy of the phase change front over longer times. Ye and Arici have recently published a series of papers dedicated to exploring many aspects of the enthalpy-porosity method through various applications. In Ye and Arici [28] they conducted 3D & 2D enthalpy-porosity simulations of pure solid-gallium phase change, comparing them with experimental results and justifying the feasibility of 3D modeling being replaced by 2D modeling. Paper Ye and Arici [29] showed novel mechanisms of convective false diffusion during modeling of the solid-liquid interface of pure solid-gallium melting. They also showcased the phenomenon of asymmetric melting for large aspect ratios founding correlations for the mean liquid layer thickness. In Ye and Arici [30] redefined interface error between numerical and experimental results and conducted thorough 2D verification and validation of enthalpy-porosity modeling of the melting process of gallium in a rectangular enclosure heated from a vertical wall. In Ye and Arici [31], a regression model for the mushy zone constant was found so that accurate modeling of calcium chloride hexahydrate convection-diffusion solid-liquid phase change could be more quickly and easily conducted with less reliance on experimental data. They also proposed a generalized expression for melting fraction vs. dimensionless time. In Ye and Arici [14] studied numerically thermal control design for applicability to a large-scale high-capacity lithium-ion energy storage system subjected to forced cooling. They were able to demonstrate increase one level batteries for the designed air gap between two adjacent modules.

In this paper, we examine the evolution of the interface between the liquid and solid phases in an infinite cylinder with either a prescribed temperature or heat flux on the outer boundary. The governing equations for the case of the prescribed temperature were derived in Barannyk, Crepeau, Paulus and Siahpush [32] where the authors assumed slow interface motion and derived a first-order nonlinear differential equation for the front's position, involving infinite Fourier Bessel-type series. Related problems for a plane wall and spherical geometry were studied in McCord et al. [33]; Williams, Barannyk, Crepeau and Paulus [34], respectively. Crepeau et al. in [35] simulated the problem in the cylindrical geometry using the method of catching of the front into a space grid node and compared their solutions with the series solutions, reporting good agreement, especially for small Stefan numbers. The problem with prescribed heat flux on the outer boundary was addressed

in Barannyk, Williams, Crepeau, Ogidan and Sakhnov [36], where the governing equations for the interface and temperature profiles were derived. Instead of using the Stefan number, which requires the temperature difference (e.g., melting temperature and outer boundary temperature), the authors introduced non-dimensional heat flux as a parameter to control heat conduction intensity inside the rod. The papers Crepeau et al. [37], McCord et al. [33]; Barannyk et al. [32]; Crepeau et al. [35]; Barannyk et al. [36]; Williams et al. [34] assume a sharp interface, meaning the transition between liquid and solid phases occurs at a point with the melting temperature, with no mushy zone considered. It was noted that both series and front catching solutions exhibited an overheating phenomenon during melting, where the temperature in the solid phase temporarily exceeded the melting temperature before the artifact disappeared. Paulus studied the problem with both prescribed temperature and the heat flux on the outer boundary in his MS thesis Paulus [38] and used the Voller and Prakesh's enthalpy-porosity finite element method Voller and Prakash [39] or shortly the enthalpy method, which is implemented into the Ansys Fluent software ANSYS, Inc [40]. The enthalpy method assumes an existence of a so-called "mushy zone" Worster [41] or a transition zone, which is a the mixed solid - liquid region, so the interface between two phases is taken to be a midpoint of the mushy zone. Paulus compared his numerical solutions with the series solutions and reported a good agreement especially during the solidification for small Stefan numbers. His enthalpy solutions did not exhibit any overheating during the melting but at the same time, the interface is computed differently with the enthalpy method compared with the sharp interface approach.

To the best of our knowledge, there are no experimental data that we could use to validate our results. Due to the challenges of conducting experimental studies, computational and analytical methods play a significant role in analysis. For this reason, we decided to systematically compare solutions obtained using different methods: the series, front catching, enthalpy as well as so-called quasi-static solutions. The enthalpy method is commonly used to solve moving boundary problems, particularly those involving phase changes like melting and solidification, because it allows for a smooth transition between phases without explicitly tracking the moving interface, making it a convenient and efficient approach in numerical simulations. For this reason, we consider solutions obtained by the enthalpy method as reference solutions. In addition, we analyzed the evolution of the mushy zone from the enthalpy simulations and compared it to the evolution of the overheated zone generated by the series and front catching methods. We found that both mushy and overheated zones have similar shape and they exist over approximately the same time interval. This suggests that the sharp

interface model is able to capture the presence of the mushy zone.

The paper is organized as follows. In [Section 2](#), we give a brief derivation of the governing equations for the interface and temperature in both phases in the case of the prescribed constant temperature at the outer boundary of the cylinder. [Section 3](#) considers the case of the prescribed heat flux at the boundary. Quasi-static solution approximation is considered in [Section 4](#). The effect of convection is discussed in [Section 5](#). The method of the catching of the front in a node is explained in [Section 6](#). The setup of the enthalpy-porosity method implemented in Ansys Fluent is given in [Section 7](#). The evolution of the interface, temperature, overheated and mushy zones are shown in [Section 8](#). [Section 9](#) provides conclusions.

2. Problem setup. The case of prescribed temperature at the boundary

We analyze the solid-liquid phase change problem in an infinite cylinder, as illustrated in [Fig. 1](#). The phase change is driven by a constant internal heat generation rate, \dot{q} , of the material. On the cylinder's outer boundary, we either impose a constant temperature T_0 , or the heat flux, q''_0 . In this section, we consider the case when the outer boundary temperature is fixed at T_0 . The case with a prescribed heat flux at the outer boundary will be addressed in the following section. Our analysis is based on the following assumptions:

1. the internal heat generation and the thermophysical properties of the materials are equal and constant in both the solid and liquid phases;

$$\eta = \frac{r}{r_0}, \quad \tau = \frac{\alpha t}{r_0^2}, \quad \theta(\eta, \tau) = \frac{T(r, t) - T_0}{T_m - T_0}, \quad \zeta = \frac{s(t)}{r_0}, \quad St = \frac{c_p(T_m - T_0)}{\Delta h_f}, \quad \dot{Q} = \frac{\dot{q}r_0^2}{k(T_m - T_0)} \quad (5)$$

2. the material undergoes phase change at a single temperature, T_m ;
3. the formation of the mushy zone is neglected, resulting in a single, distinct interface between the phases, or so-called a sharp interface;
4. there is no temperature variation circumferentially in the cylinder, meaning heat transfer occurs solely in the radial direction;
5. all forms of convection are considered negligible. The effect of convection will be discussed in [Section 5](#).

Energy transfer in the cylinder is described by the heat equation with internal heat generation in cylindrical coordinates, as given by Incropera and DeWitt [\[42\]](#),

$$\frac{1}{r} \frac{\partial}{\partial r} \left(r \frac{\partial T}{\partial r} \right) + \frac{\dot{q}}{k} = \frac{1}{\alpha} \frac{\partial T}{\partial t}, \quad T = T(r, t), \quad 0 \leq s \leq r_0, \quad 0 \leq t \leq \infty \quad (1)$$

where $r = 0$ corresponds to the centerline of the cylinder and $r = r_0$ its outside boundary. Along the interface between the solid and liquid

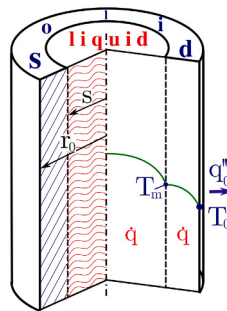


Fig. 1. Schematic diagram of the phase change problem in a cylindrical geometry.

phases, an energy balance yields Poulikakos [\[43\]](#),

$$k \frac{\partial T_{liq}(r, t)}{\partial r} \Big|_{r=s(t)} + \rho \Delta h_f \frac{ds(t)}{dt} = k \frac{\partial T_{sol}(r, t)}{\partial r} \Big|_{r=s(t)} \quad (2)$$

With constant surface temperature boundary condition, the temperature at the surface $r = r_0$ is imposed to be T_0 .

To close the system, one needs to prescribe the boundary and initial conditions. In the liquid phase, they are,

$$\frac{\partial T_{liq}(r, t)}{\partial r} \Big|_{r=0} = 0, \quad T_{liq}(s(t), t) = T_m, \quad T_{liq}(r, 0) = \phi_{liq}(r) \quad (3)$$

The first boundary condition represents symmetry of the problem with respect to the centerline located at $r = 0$ since we expect a parabolic profile of the temperature [\[44\]](#).

The boundary conditions and initial condition in the solid phase are,

$$T_{sol}(s(t), t) = T_m, \quad T_{sol}(r_0, t) = T_0, \quad T_{sol}(r, 0) = \phi_{sol}(r) \quad (4)$$

The second boundary condition in (3) along with the first boundary condition in (4), implies that the temperature is continuous across the interface $r = s(t)$.

The governing equations for the interface and temperature in both phases were derived in Barannyk et al. [\[32\]](#). We provide the main steps in the derivation. For details, please refer to the above paper. We start with nondimensionalizing the problem and introducing the following dimensionless variables:

Since the specific heat c_p and the latent heat of fusion Δh_f are fixed, the Stefan number St is a linear function of the difference between the melting temperature T_m at the front and the prescribed temperature T_0 at the outer boundary. Consequently, the Stefan number St is small when temperature variations are small and increases with greater temperature contrast.

Introducing dimensionless variables into the heat Eq. (1) and boundary and initial conditions ((3) and (4)) results in dimensionless heat equation,

$$\frac{1}{\eta} \frac{\partial}{\partial \eta} \left(\eta \frac{\partial \theta}{\partial \eta} \right) + \dot{Q} = \frac{\partial \theta}{\partial \tau}, \quad 0 \leq \eta \leq 1, \quad \tau \geq 0 \quad (6)$$

with the corresponding dimensionless boundary and initial conditions specified in the liquid and solid regions, respectively, as,

$$\frac{\partial \theta_{liq}(0, \tau)}{\partial \eta} = 0, \quad \theta_{liq}(\zeta(\tau), \tau) = 1, \quad \theta_{liq}(\eta, 0) = \Phi_{liq}(\eta) \quad (7)$$

$$\theta_{sol}(\zeta(\tau), \tau) = 1, \quad \theta_{sol}(1, \tau), \quad \theta_{sol}(\eta, 0) = \Phi_{sol}(\eta) \quad (8)$$

Here Φ_{liq} and Φ_{sol} denote the initial dimensionless temperature profiles in the liquid and solid phases, respectively. The interface Eq. (2) transforms to,

$$\frac{\partial \theta_{liq}}{\partial \eta} \Big|_{\eta=\zeta(\tau)} + \frac{1}{St} \frac{d\zeta}{d\tau} = \frac{\partial \theta_{sol}}{\partial \eta} \Big|_{\eta=\zeta(\tau)} \quad (9)$$

Problem (6)–(9) is a coupled initial boundary value problem for the second order partial differential equation. One approach is to solve this problem completely numerically using the methods for partial differential equations. We use the finite difference method of catching of a front into a node Samarskii and Vabishchevich [\[45\]](#) and the finite

element enthalpy method Voller and Prakash [39] to numerically solve the problem. Another approach is to use analytical methods to reduce the given problem to a problem that involves a first order ordinary differential equation in time that can be solved numerically using standard initial value problem solvers. In particular, we use the method of separation of variables to find temperature in each phase and then substitute θ_{liq} and θ_{sol} into the interface Eq. (9) to find the evolution equation of the front $\zeta(\tau)$. Given that the front's position depends on time, to apply the method of separation of variables, we assume that the front moves slowly relatively to the evolution of the temperature within each phase. We call the interface weakly time dependent. This approach extends the approach used in Crepeau and Siahpush [7] where the front was considered to be time dependent but the temperature in each phase was solely depended on the spatial variable, which resulted in so-called quasi-static solution.

We begin by solving the problem in the liquid phase. Due to the nonhomogeneous nature of the heat Eq. (6), we decompose the solution θ_{liq} into transient and quasi steady-state components Poulikakos [43]; Haberman [46], Kreyszig [47]

$$\theta_{liq}(\eta, \tau) = \theta_{liq,tr}(\eta, \tau) + \theta_{liq,ss}(\eta), \quad 0 < \eta < \zeta(\tau) \quad (10)$$

We use the term "quasi" since the position of the front $\zeta(\tau)$ depends on time τ , albeit in a weakly time-dependent manner. This allows us to treat quasi steady-state solution as if it were a steady-state solution. We substitute the sum of temperature components (10) into the heat Eq. (6) and the boundary and initial conditions (7). Using the linearity, the problem is then split into the transient and quasi steady-state problems. The transient part consists of the homogeneous heat equation,

$$\frac{1}{\eta} \frac{\partial}{\partial \eta} \left(\eta \frac{\partial \theta_{liq,tr}}{\partial \eta} \right) = \frac{\partial \theta_{liq,tr}}{\partial \tau} \quad (11)$$

with the homogeneous boundary and corresponding initial conditions,

$$\frac{\partial \theta_{liq,tr}(0, \tau)}{\partial \eta} = 0, \quad \theta_{liq,tr}(\zeta(\tau), \tau) = 0, \quad \theta_{liq,tr}(\eta, 0) = \Phi_{liq}(\eta) - \theta_{liq,ss}(\eta) \quad (12)$$

The quasi steady-state portion satisfies the nonhomogeneous steady-state heat equation,

$$\frac{1}{\eta} \frac{d}{d\eta} \left(r \frac{d\theta_{liq,ss}}{d\eta} \right) = -\dot{Q} \quad (13)$$

with boundary conditions,

$$\frac{d\theta_{liq,ss}(0)}{d\eta} = 0, \quad \theta_{liq,ss}(\zeta(\tau)) = 1 \quad (14)$$

and can be directly integrated to find

$$\theta_{liq,ss}(\eta) = \frac{1}{4} \dot{Q} (\zeta^2 - \eta^2) + 1 \quad (15)$$

For the transient portion $\theta_{liq,tr}(\eta, \tau)$ of the temperature in the liquid phase, we use the method of separation of variables to find that the time dependent part is the exponentially decaying function $e^{-\lambda^2 \tau}$, where λ is an eigenvalue. The spatial part of the solution satisfies the Bessel equation of order 0 whose linearly independent solutions are $J_0(\lambda\eta)$ and $Y_0(\lambda\eta)$, the Bessel functions of the first and second kind of order 0, respectively. Since the liquid phase includes the centerline $\eta = 0$ (in dimensionless variables) and Y_0 is unbounded at the origin, only function $J_0(\lambda\eta)$ contributes to the solution. Applying the boundary condition $\frac{\partial \theta_{liq,tr}(0, \tau)}{\partial \eta} = 0$, we find the eigenvalues

$$\lambda_n = \frac{z_{0n}}{\zeta(\tau)}, \quad n = 1, 2, \dots \quad (16)$$

where z_{0n} are the zeros of the Bessel function J_0 . The associated eigen-

functions are $J_0(\lambda_n \eta)$. These functions are orthogonal on the interval $[0, \zeta]$ with respect to the weight η , as per the Sturm-Liouville theory Haberman [46].

The principle of linear superposition then provides the transient temperature profile in the liquid phase as

$$\theta_{liq,tr}(\eta, \tau) = \sum_{n=1}^{\infty} A_n e^{-\lambda_n^2 \tau} J_0(\lambda_n \eta) \quad (17)$$

To find coefficients A_n , we use the initial conditions in (12) and orthogonality of the eigenfunctions $J_0(\lambda_n \eta)$, to get

$$A_n = \frac{\int_0^{\zeta(\tau)} [\Phi_{liq}(\eta) - \theta_{liq,ss}(\eta)] J_0(\lambda_n \eta) \eta d\eta}{\int_0^{\zeta(\tau)} J_0^2(\lambda_n \eta) \eta d\eta} \quad (18)$$

Therefore, by combining the solutions (15) and (17), the complete temperature profile in the liquid phase becomes,

$$\theta_{liq}(\eta, \tau) = \sum_{n=1}^{\infty} A_n e^{-\lambda_n^2 \tau} J_0(\lambda_n \eta) + \frac{1}{4} \dot{Q} (\zeta^2 - \eta^2) + 1 \quad (19)$$

with A_n and λ_n defined in (18) and (16), respectively. The choice of the initial conditions will be discussed later.

A similar process applies to the solid phase. The temperature profile in the solid is also separated into transient and quasi steady-state parts. Direct integration is employed to calculate the quasi steady-state portion of the temperature in the solid phase:

$$\theta_{sol,ss}(\eta) = \frac{1}{4} \dot{Q} (1 - \eta^2) + \left(\frac{1}{4} \dot{Q} (\zeta(\tau) - 1) + 1 \right) \frac{\ln \eta}{\ln \zeta(\tau)} \quad (20)$$

The transient problem is again the homogeneous heat equation,

$$\frac{1}{\eta} \frac{\partial}{\partial \eta} \left(\eta \frac{\partial \theta_{sol,tr}}{\partial \eta} \right) = \frac{\partial \theta_{sol,tr}}{\partial \tau} \quad (21)$$

with the homogeneous boundary and corresponding initial conditions,

$$\frac{\partial \theta_{sol,tr}(0, \tau)}{\partial \eta} = 0, \quad \theta_{liq,tr}(\zeta(\tau), \tau) = 0, \quad \theta_{sol,tr}(\eta, 0) = \Phi_{liq}(\eta) - \theta_{liq,ss}(\eta) \quad (22)$$

Similar to the approach used in the liquid phase, we employ separation of variables to solve the initial value boundary problem defined by Eqs. (21) and (22). Since the solid phase is away from the centerline $\eta = 0$, both Bessel functions $J_0(\lambda\eta)$ and $Y_0(\lambda\eta)$ are part of the solution. Boundary conditions from (22) yield the equation:

$$F(\tilde{\lambda}, \zeta) \equiv J_0(\tilde{\lambda}\zeta(\tau)) Y_0(\tilde{\lambda}) - Y_0(\tilde{\lambda}\zeta(\tau)) J_0(\tilde{\lambda}) = 0 \quad (23)$$

The zeroes of the function $F(\tilde{\lambda}, \zeta)$ represent the eigenvalues of the problem in the solid phase, denoted by $\tilde{\lambda}_n$. There are infinitely many roots, which we compute numerically using the Matlab function `fzero`. This function implements an algorithm developed by T. Dekker, combining bisection, secant, and inverse quadratic interpolation methods Dekker [48]; Dekker and Hoffmann [49]; Moler [50]. To find a root, one must provide an interval where the root is expected to be located. To determine such an interval, we use asymptotic approximations of the Bessel functions applicable for large z Haberman [46]:

$$J_n(z) \simeq \sqrt{\frac{2}{\pi z}} \cos\left(z - \frac{\pi n}{2} - \frac{\pi}{4}\right), \quad Y_n(z) \simeq \sqrt{\frac{2}{\pi z}} \sin\left(z - \frac{\pi n}{2} - \frac{\pi}{4}\right), \quad z \rightarrow \infty \quad (24)$$

because their roots can be readily determined, thus:

$$\tilde{\lambda}_n \approx \tilde{\lambda}_n^{as} = \frac{-\frac{\pi}{2} + \pi n}{1 - \zeta}, \quad n = 1, 2, \dots$$

The roots $\tilde{\lambda}_n^{as}$ can serve as centers for intervals where the roots $\tilde{\lambda}_n$ are located. The function $F(\tilde{\lambda}, \zeta)$ is quasi-periodic, and the spacing between

successive roots approaches a constant as n increases. Approximately a half or a quarter of the distance between successive roots can define the interval centered at $\tilde{\lambda}_n^{as}$ within which the root $\tilde{\lambda}_n$ will be computed using the function *fzero*. The asymptotic approximations (24) become increasingly accurate for large arguments z but they still provide a reliable approximation even for the smallest root $\tilde{\lambda}_1$.

Once the eigenvalues $\tilde{\lambda}_n$ are determined, we can write the corresponding eigenfunctions,

$$f_n(\eta) = Y_0(\tilde{\lambda}_n\eta) - \frac{Y_0(\tilde{\lambda}_n)}{J_0(\tilde{\lambda}_n)} J_0(\tilde{\lambda}_n) \quad (25)$$

of the Sturm-Liouville boundary value problem on the interval $[\zeta, 1]$ [Haberman [46]].

The principle of linear superposition provides the transient part of the temperature in the solid phase as:

$$\theta_{tr,sol}(\eta, \tau) = \sum_{n=1}^{\infty} B_n f_n(\eta) e^{-\tilde{\lambda}_n^2 \tau} \quad (26)$$

The coefficients B_n can be computed by using the initial condition in (22) together with the orthogonality of eigenfunctions f_n on $[\zeta, 1]$ with respect to the weight function η [Haberman [46]]:

$$B_n = \frac{\int_{\zeta(\tau)}^1 [\Phi_{sol}(\eta) - \theta_{ss,sol}(\eta)] f_n(\eta) \eta d\eta}{\int_{\zeta(\tau)}^1 f_n^2(\eta) \eta d\eta} \quad (27)$$

Therefore, the temperature distribution in the solid is given by,

$$\theta_{sol}(\eta, \tau) = \sum_{n=1}^{\infty} B_n f_n(\eta) e^{-\tilde{\lambda}_n^2 \tau} + \frac{1}{4} \dot{Q}(1 - \eta^2) + \left(\frac{1}{4} \dot{Q}(\zeta(\tau) - 1) + 1 \right) \frac{\ln \eta}{\ln \zeta(\tau)} \quad (28)$$

with $f_n(\eta)$ and B_n are defined in Eqs. (25) and (27), respectively, and the eigenvalues $\tilde{\lambda}_n$ are the roots of Eq. (23). Eqs. (19) and (28) provide the temperature profiles in the liquid and solid phases, respectively. From those relations, the temperature gradients can be calculated and evaluated at the front $\eta = \zeta(\tau)$, and then inserted into the interface Eq. (9). Thus, we obtain the following first-order ordinary differential equation governing the motion of the interface, $\zeta(\tau)$:

$$\begin{aligned} \frac{1}{St} \frac{d\zeta(\tau)}{d\tau} &= \sum_{n=1}^{\infty} \lambda_n A_n J_1(\lambda_n \zeta(\tau)) e^{-\tilde{\lambda}_n^2 \tau} - \sum_{n=1}^{\infty} \tilde{\lambda}_n B_n e^{-\tilde{\lambda}_n^2 \tau} \left[Y_1(\tilde{\lambda}_n \zeta(\tau)) - \frac{Y_0(\tilde{\lambda}_n)}{J_0(\tilde{\lambda}_n)} \right] \\ &+ \left(\frac{\dot{Q}}{4} (\zeta^2(\tau) - 1) + 1 \right) \frac{1}{\zeta(\tau) \ln \zeta(\tau)} \end{aligned} \quad (29)$$

To determine the evolution of the interface $\zeta(\tau)$ over time τ , we solve Eq. (29) numerically using the *ode23* solver in Matlab, which is based on a modified Rosenbrock formula of order 2 Shampine and Reichelt [51]. To simulate the melting process, we use the initial conditions,

$$\Phi_{liq}(\eta) = 1, \quad \Phi_{sol}(\eta) = 1 - \eta^2, \quad \zeta(0) = 0 \quad (30)$$

The corresponding initial conditions for solidification are:

$$\Phi_{liq}(\eta) = \frac{\dot{Q}}{4} (1 - \eta^2) + 1, \quad \Phi_{sol}(\eta) = 1, \quad \zeta(0) = 1 \quad (31)$$

The initial temperature distributions are based on the parabolic profiles, typical for heat transfer problems with internal heat generation. Once the position of the interface is known, it can be used in (19) and (28) to find the corresponding temperatures in the liquid and solid phase, respectively. Since the eigenvalues in both phases are positive and the temperatures decay exponentially over time at rates determined by the eigenvalues, only a few terms are needed in the simulations. We find that 5–10 terms is sufficient to accurately represent the temperatures and the right-hand side of the evolution Eq. (29).

3. Problem setup. The case of prescribed heat flux at the boundary

In this case, instead of prescribing a fixed constant temperature T_0 at the outer boundary $r = r_0$, we prescribe a constant heat flux q''_0 . The schematic of the problem remains the same as in Fig. 1. We also assume that the thermophysical properties of the materials are the same in both phases, that the phase change occurs at a single point at the melting temperature T_m , implying a sharp interface approach with no mushy zone, and that the phase change is driven by the internal heat generation \dot{Q} .

The governing equations consist of the same heat Eq. (1) throughout the domain $0 \leq r \leq r_0$ and the energy Eq. (2) at the interface $\eta = \zeta(\tau)$. The boundary and initial conditions in the liquid phase remain the same as in (3). In the solid case, the boundary and initial conditions are the same as in (4) except that instead of $T_{sol}(r_0, t) = T_0$ we impose a constant heat flux $-k \frac{\partial T_{sol}(r, t)}{\partial r} \Big|_{r=r_0} = q''_0$.

In the case of a prescribed constant temperature at $r = r_0$, there were two temperatures: the melting temperature T_m and the prescribed temperature T_0 at $r = r_0$. This allowed us to introduce the Stefan number St , which depended on the temperature difference $T_m - T_0$. However, in the case of a prescribed heat flux at the outer boundary, there is only one fixed temperature: T_m . Therefore, it is more convenient to use a slightly different non-dimensionalization and introduce a dimensionless heat flux Q'' on the outer boundary instead of St . We have the following dimensionless variables and groups:

$$\begin{aligned} \eta &= \frac{r}{r_0}, \quad \zeta = \frac{s(t)}{r_0}, \quad \tau = \frac{at}{r_0^2}, \quad \theta(\eta, \tau) = \frac{T(r, t) - T_m}{T^*}, \quad \dot{Q} = \frac{\dot{q} r_0^2}{\alpha \rho \Delta h_f}, \quad Q'' = \frac{q'' r_0}{\alpha \rho \Delta h_f} \\ \Phi_{liq}(\eta) &= \frac{\phi_{liq}(r_0 \eta) - T_m}{T^*}, \quad \Phi_{sol}(\eta) = \frac{\phi_{sol}(r_0 \eta) - T_m}{T^*} \end{aligned}$$

where $T^* = \frac{\alpha \rho \Delta h_f}{k}$ is a characteristic temperature obtained by balancing the second and third terms in the interface Eq. (2).

In dimensionless form, the governing equations, along with boundary and initial conditions, are as follows:

$$\begin{aligned} \frac{\partial^2 \theta(\eta, \tau)}{\partial \eta^2} + \dot{Q} &= \frac{\partial \theta(\eta, \tau)}{\partial \tau}, \quad 0 \leq \eta \leq 1, \quad \tau \geq 0 \\ \frac{\partial \theta_{liq}(0, \tau)}{\partial \eta} &= 0, \quad \theta_{liq}(\zeta(\tau), \tau) = 0, \quad \theta_{liq}(\eta, 0) = \Phi_{liq}(\eta), \quad 0 \leq \eta \leq \zeta(\tau) \end{aligned} \quad (32)$$

$$\begin{aligned} \theta_{sol}(\zeta(\tau), \tau) &= 0, \quad \frac{\partial \theta_{sol}(\eta \tau)}{\partial \eta} \Big|_{\eta=1} = -Q'', \quad \theta_{sol}(\eta, 0) = \Phi_{sol}(\eta), \quad \zeta(\tau) \leq \eta \leq 1 \\ \frac{\partial \theta_{liq}(\eta \tau)}{\partial \eta} \Big|_{\eta=\zeta} + \frac{d\zeta(\tau)}{d\tau} &= \frac{\partial \theta_{sol}(\eta \tau)}{\partial \eta} \Big|_{\eta=\zeta}, \quad 0 \leq \zeta \leq 1 \end{aligned} \quad (33)$$

As evident from the dimensionless interface Eq. (33), the Stefan number is not present. Instead, the boundary condition in the solid phase at $\eta = 1$ is linked to another dimensionless parameter: the heat flux Q'' . By keeping \dot{Q} fixed and adjusting Q'' , we control the amount of heat extracted at the outer boundary.

Applying a similar methodology as in the case with a prescribed temperature at the outer boundary, we address a nonhomogeneous problem by decomposing the solution into a transient and quasi steady-state components. We employ the method of separation of variables, assuming that the front ζ moves relatively slowly compared to the temperature evolution in each phase, to derive the transient solution and the quasi steady-state component. In the liquid phase, the temperature is

$$\theta_{liq}(\eta, \tau) = \sum_{n=1}^{\infty} \widetilde{A}_n e^{-\tilde{\lambda}_n^2 \tau} J_0(\tilde{\lambda}_n \eta) + \frac{\dot{Q}}{4} (\zeta^2(\tau) - \eta^2), \quad 0 \leq \eta \leq \zeta \quad (34)$$

where

$$\tilde{A}_n = \frac{\int_0^{\zeta(\tau)} [\Phi_{liq}(\eta) - \theta_{liq,ss}(\eta)] J_0(\hat{\lambda}_n \eta) \eta d\eta}{\int_0^{\zeta(\tau)} J_0^2(\hat{\lambda}_n \eta) \eta d\eta}$$

Here, $\hat{\lambda}_n = \frac{z_{0n}}{\zeta(\tau)}$ represent eigenvalues with associated eigenfunctions $f_n(\eta) = J_0(\hat{\lambda}_n \eta)$, where $J_0(z)$ denotes the Bessel function of the 1st kind of order 0, and z_{0n} are zeros of $J_0(z)$ for $n = 1, 2, 3, \dots$. The solution in (34) closely resembles (19) from the previous section, with the distinction that the absence of a constant 1 arises from different non-dimensionalization choices. In the case of a prescribed constant temperature, the dimensionless variables are selected such that the dimensionless temperature at the front is set to 1, whereas for a prescribed heat flux, the temperature at the front is set to 0. More details can be found in Barannyk et al. [36].

In the solid phase, where $\zeta \leq \eta \leq 1$, the temperature is,

$$\theta_{sol}(\eta, \tau) = \sum_{n=1}^{\infty} \tilde{B}_n e^{-\hat{\lambda}_n^2 \tau} \tilde{f}_n(\eta) + \frac{\dot{Q}}{4} (\zeta^2(\tau) - \eta^2) + \left(\frac{\dot{Q}}{2} - Q'' \right) \ln \frac{\eta}{\zeta(\tau)}, \quad \zeta \leq \eta \leq 1 \quad (35)$$

where the eigenvalues $\hat{\lambda}_n$, for $n = 1, 2, 3, \dots$, are roots of the equation

$$J_0(\tilde{\lambda}\zeta) Y_1(\tilde{\lambda}) - Y_0(\tilde{\lambda}\zeta) J_1(\tilde{\lambda}) = 0$$

with associated eigenfunctions

$$\tilde{f}_n(\eta) = J_0(\tilde{\lambda}_n \eta) - \frac{J_1(\tilde{\lambda}_n)}{Y_1(\tilde{\lambda}_n)} Y_0(\tilde{\lambda}_n \eta)$$

and Fourier-Bessel coefficients are

$$\tilde{B}_n = \frac{\int_{\zeta(\tau)}^1 [\Phi_{sol}(\eta) - \theta_{sol,ss}(\eta)] \tilde{f}_n(\eta) \eta d\eta}{\int_{\zeta(\tau)}^1 \tilde{f}_n^2(\eta) \eta d\eta}$$

$J_1(z)$, $Y_1(z)$ are Bessel functions of the 1st and 2nd kind of order 1.

By differentiating $\theta_{liq}(\eta, \tau)$ and $\theta_{sol}(\eta, \tau)$ with respect to η , evaluating these derivatives at the front $\eta = \zeta(\tau)$, using the identities

$$J'_0(z) = -J_1(z), \quad Y'_0(z) = -Y_1(z)$$

and then substituting the resulting expressions into the interface Eq. (33), we find the equation for the front $\zeta(\tau)$,

$$\frac{d\zeta}{d\tau} = \sum_{n=1}^{\infty} \tilde{A}_n \hat{\lambda}_n e^{-\hat{\lambda}_n^2 \tau} J_1(\hat{\lambda}_n \zeta) + \sum_{n=1}^{\infty} \tilde{B}_n \hat{\lambda}_n e^{-\hat{\lambda}_n^2 \tau} \tilde{f}_n(\zeta) + \left(\frac{\dot{Q}}{2} - Q'' \right) \frac{1}{\zeta} \quad (36)$$

where

$$\tilde{f}_n(\eta) = -J_1(\hat{\lambda}_n \eta) + \frac{J_1(\hat{\lambda}_n)}{Y_1(\hat{\lambda}_n)} Y_1(\hat{\lambda}_n \eta)$$

Eq. (36) is an ordinary differential equation for $\zeta = \zeta(\tau)$ and can be solved numerically to compute the evolution of the interface using ODE solvers. Then Eqs. (34) and (35) can be used to find temperature in both phases. Due to the rapid temporal decay, it is sufficient to retain only a few terms in the infinite series to achieve accurate approximations.

4. Quasi-static solutions

4.1. Prescribed temperature case

The quasi-static approximation assumes that the temperature has negligible temporal variation, while the front position depends on time.

Crepeau et al. Crepeau and Siahpush [7] employed this method to address the Stefan problem with internal heat generation in various geometries. Using the quasi steady-state temperature profiles (Eqs. (15) and (20)) in the interface Eq. (9) yields,

$$\frac{1}{St} \frac{d\zeta}{d\tau} = \frac{4 + \dot{Q}(\zeta^2 - 1)}{4\zeta \ln \zeta} \quad (37)$$

This Eq. (37) is particularly useful for determining steady-state behavior, which occurs when $\frac{d\zeta}{d\tau} = 0$. Solving the resulting algebraic equation yields,

$$\zeta_{ss} = \sqrt{1 - \frac{4}{\dot{Q}}} \quad (38)$$

This expression provides two key results: (1) the minimum value for \dot{Q} is 4, and the condition for an non-static front is $\dot{Q} > 4$; and (2) for the \dot{Q} used in this paper ($\dot{Q} = 5$), the steady-state interface position is $\zeta_{ss} \approx 0.45$. This implies that, starting from any initial condition, the front position should approach the values of 0.45 as time increases.

4.2. Prescribed heat flux case

The quasi-static solution in this case can be obtained from Eq. (36) by letting $\tau \rightarrow \infty$ to reach the steady-state solutions. This yields,

$$\frac{d\zeta}{d\tau} = \left(\frac{\dot{Q}}{2} - Q'' \right) \frac{1}{\zeta} \quad (39)$$

Integrating this equation and using the initial condition $\zeta(0) = \zeta_0$, we find:

$$\zeta(\tau) = \sqrt{(\dot{Q} - 2Q'')\tau + \zeta_0^2} \quad (40)$$

The result in (40) suggests that the interface ζ behaves like $\tau^{1/2}$, which is consistent with the findings in Crepeau and Siahpush [7]. Eq. (39) also implies that to promote melting, $\frac{d\zeta}{d\tau}$ should be positive, since the front has to move from the centerline to the right, so $Q'' < \frac{\dot{Q}}{2}$ should be required. Conversely, for solidification, $\frac{d\zeta}{d\tau}$ should be negative, necessitating $Q'' > \frac{\dot{Q}}{2}$.

5. Justification of neglecting convection

In this section, we analyze if the convection can be disregarded during melting using nuclear fuel rods as an illustrative example. As it is well known, the Nusselt number Nu quantifies the ratio of convective to conductive heat transfer. For a free convective flow, this parameter can be calculated by the Elenbaas formula Elenbaas [52],

$$Nu = \frac{1}{24} Ra_m \left[1 - \exp \left(-\frac{35}{Ra_m} \right) \right]^{3/4} \quad (41)$$

This formula is taken from papers Terekhov and Ekaid [53], Terekhov, Ekaid and Yassin [54] after correcting the sign in the exponent. It is valid for free convection in vertical parallel plate configurations and can be applied to cylindrical configurations as the gravity vector would not cross two cylindrical shells sharing an origin. The modified Rayleigh number Ra_m is given by $Ra_m = Ra \frac{\omega}{L}$, where $\omega = D/2 \cdot \zeta$ represents the distance from the center of the rod to the melting front, with D as the rod diameter, and ζ denoting the non-dimensional coordinate of the melting front, and L is the length of the rod. The classical definition of the Rayleigh number is:

$$Ra = \frac{\rho^2 c_p \beta \Delta T \omega^3}{\mu k} \quad (42)$$

where ρ is the liquid density, c_p is the heat capacity, β is the volume

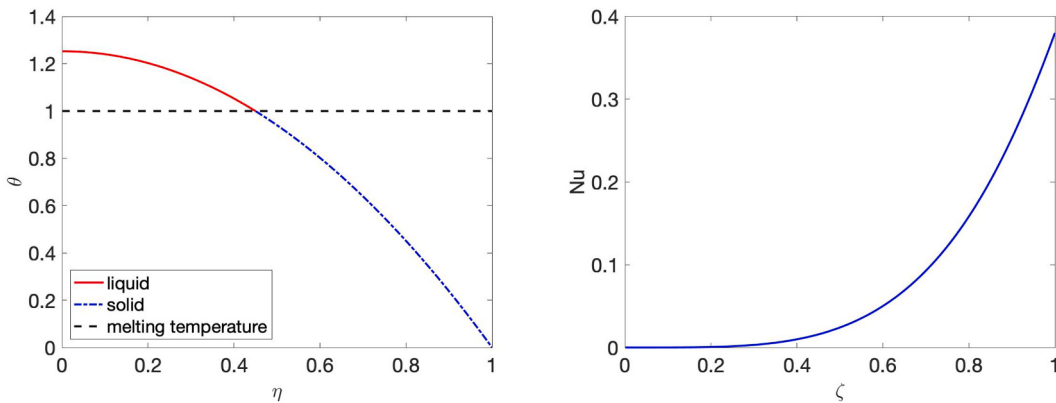


Fig. 2. A non-dimensional steady-state temperature distribution of partially melted rod (left). Nusselt number Nu as a function of the front ζ (right).

expansion coefficient, μ is the dynamic viscosity, and k is the thermal conductivity. Since convection can only occur in the liquid phase, the temperature difference ΔT is set as the difference between the temperature T_c at the center of the rod and the melting temperature T_m at the front:

$$\Delta T = T_c - T_m \quad (43)$$

Fig. 2 on the left demonstrates the non-dimensional temperature distribution of a partially melted rod in the steady state in the case of the prescribed temperature at the outer boundary. At the center of rod ($\eta = 0$), non-dimensional temperature equals 1.25. Non-dimensional temperature θ is defined in Eq. (5).

To evaluate the effect of convection, we use the actual parameters of a uranium dioxide rod from a WWER-1000 nuclear reactor Zheleznjak, Panjushkin, Sharikov, Bek, Doronin, Duhovenskij, Bibilashvili, Mezhuev, Lavrenjuk, Rozhkov, Enin, Popozov and Kushmanov [55]; Andrushevko, Afrov, Vasiliev, Generalov, Kosourov, Semchenkov and Ukrainstsev [56]:

$$T_0 = 1173K, \quad D = 7.57 \cdot 10^{-3}m, \quad L = 3.35m \quad (44)$$

Taking into account the melting temperature of uranium dioxide, $T_m = 3173K$ Kirillov and Bogoslovskaya [57], and using the formula for non-dimensional temperature (Eq. (5)), we solve for T_c numerically using the method of catching of the front into a space grid node (discussed in Section 6) at the steady state: $T_c = 3610.5K$. The appropriate thermo-physical properties for liquid uranium dioxide can be obtained from Kirillov and Bogoslovskaya [57] for the slightly higher central temperature of $T_c = 3673K$, as the data are tabulated in increments of 100 K. They are given in Table 1.

Fig. 2 on the right shows the Nusselt number Nu as a function of the front position ζ within the rod. The temperature difference was calculated using the catching of the front method with only conduction. This approach is valid because convection would facilitate heat transfer, resulting in a smaller temperature difference and a lower Nusselt number. Thus, using a model with just conduction overestimates the significance of convection. The graph of the Nusselt number Nu shows that in the steady-state regime: $\zeta \approx 0.45$ (determined by the quasi-static approximation in Section 4), $Nu \approx 0.017$. This indicates that the convective heat transfer is only 1.7 % of the conductive heat transfer. Consequently, we can neglect free convection during considerations of a

Table 1
Thermo-physical properties for liquid uranium dioxide.

ρ	c_p	k at $T = 3473K$	μ	β
$\frac{kg}{m^3}$	$J/kg \cdot K$	$W/m \cdot K$	$Pa \cdot s$	$\frac{1}{K}$

melted rod in the problems with a prescribed temperature at the outer boundary.

In the case of a prescribed heat flux at $r = r_0$, there is no steady state, and the front reaches the outer boundary in less than a second in the examples considered (see Fig. 9 where the dimensional times $t = \frac{r_0^2}{\alpha} \tau$ for reaching the outer boundary for $Q' = 1.5, 2.0$ and 2.4 are 0.04 s, 0.08 s and 0.42 s, respectively). Thus, the effects of convection may be neglected.

6. The method of catching of the front into a space grid node

The problem under consideration was also solved by the method of catching of the front into a space grid node, a technique introduced by Samarskii and Vabishchevich in Samarskii and Vabishchevich [45]. This method discretizes space with a uniform space grid $\Delta\eta$. The time step $\Delta\tau$ is calculated so that the front moves exactly one spatial grid size $\Delta\eta$, in other words, $\Delta\tau$ is the time it takes for the front to move from one space node to the next. This time step can be derived from the interface Eq. (9) by expanding temperature in a Taylor series in space and using the second derivative provided by the nonhomogenous heat Eq. (6):

$$\Delta\tau = \frac{\frac{\Delta\eta^2}{2}(a+b)(\theta_m - \theta_{i-1,j}) + \frac{\Delta\eta}{St}}{b(\theta_{i,j+1} - \theta_m) - a(\theta_m - \theta_{i,j-1}) + \dot{Q}\frac{\Delta\eta^2}{2}(a+b)}, \quad a = \frac{1}{\Delta\eta + \frac{\Delta\eta^2}{2\eta}}, \quad b = \frac{1}{\Delta\eta - \frac{\Delta\eta^2}{2\eta}} \quad (45)$$

The time step depends on the front position and the temperature in each phase. After discretization, the temperature at spatial nodes satisfies a linear system, which is solved at each time step using the iterative Thomas algorithm described in Anderson et al. [58], Pletcher et al. [59]. The results of numerical simulations using the front-catching method and the series solution derived in Section 2 were presented by Crepeau et al. Crepeau et al. [35]. The authors demonstrated that, except for early times at large Stefan numbers, the series solution closely matched the front-catching solution.

7. Enthalpy-porosity method

The enthalpy-porosity method, often referred to simply the enthalpy method, models the phase change front with a mushy zone, which is a mixed solid–liquid region, by introducing a specific enthalpy function H . In the mushy zone, the enthalpy, a thermodynamic state variable that measures overall heat, is not constant. Instead, it increases with the liquid fraction. While there are several implementations of the enthalpy method Voller [60], we use the enthalpy-porosity method developed by Voller and Prakash Voller and Prakash [39]. This model employs a variation of the energy equation:

$$\frac{\partial}{\partial t}(\rho H) + \nabla \cdot (\rho \vec{v} H) = \nabla \cdot (k \nabla T) + S \quad (46)$$

where H is a sum of the sensible heat, h , and the latent heat, ΔH ; ρ is the material density; \vec{v} is the fluid velocity field; and S is the source term due to the internal heat generation. The sensible heat is related to temperature through specific heat:

$$h = h_{ref} + \int_{T_{ref}}^T c_p dT \quad (47)$$

where h_{ref} is the reference enthalpy at the reference temperature T_{ref} . The latent heat ΔH is connected to the latent heat of fusion Δh_f and liquid fraction β :

$$\Delta H = f(T) = \begin{cases} \Delta h_f & \text{for } T > T_m \\ \Delta h_f \beta & \text{for } T = T_m \\ 0 & \text{for } T < T_m \end{cases} \quad (48)$$

For pure metals, liquid fraction is solved for by inverting Eq. (48), and by multiplying by c_p , we recover the sensible heat Voller and Prakash [39]; ANSYS, Inc [40]; Paulus [38]:

$$h = c_p \cdot f^{-1}(\Delta H)$$

Velocity can be solved using an appropriate set of flow equations; however, in our case, we can assume a zero velocity field as we neglect the convection effect.

The enthalpy-porosity method is implemented in the commercially available CFD package Ansys Fluent ANSYS, Inc [40].

8. Results and discussion

In this section, we compare the series solutions derived in Sections 2 and 3, the front catching solutions (Section 6), and the enthalpy-porosity solutions (Section 7) for both prescribed temperature and heat flux at the outer boundary. We also compute the evolution of the mushy and overheated zones and use that information to explain discrepancies between the solutions. We refer to the quasi-static solution to compare it with the performance of the series solution.

In our numerical experiments, we set the internal heat generation to $\dot{Q} = 5$. For the prescribed temperature at the outer boundary, we use Stefan numbers $St = 0.01, 0.1, 1$ and 10 . The series and quasi-static solutions were presented in Barannyk et al. [32], while the front catching solutions were compared to the series solutions in Crepeau et al. [35]. The enthalpy solutions were obtained by Paulus in his MS thesis Paulus [38], where he demonstrated that the enthalpy solutions did not exhibit any overheating during melting, unlike the series solutions.

For the prescribed heat flux at the outer boundary, we still fix the internal heat generation at $\dot{Q} = 5$ but vary the heat flux Q'' at the outer boundary. The series and front catching temperature profiles and interface evolution were shown in Barannyk et al. [36]. The overheating artifacts were reported but no attempt was made to explain the presence of the overheated zone. In this section, we systematically compare semi-analytical and numerical solutions obtained by the above methods, investigate the evolution of the mushy zone obtained by the enthalpy method, and compare it with the evolution of the overheated zone using the series and the front catching solutions.

8.1. Prescribed temperature case

In Fig. 3, we show the evolution of the interface during the melting (left) and solidification (right). The series and front catching solutions exhibit excellent agreement for smaller Stefan numbers $St = 0.01$ and 0.1 , but the series solution reaches the steady-state slightly faster than other solutions for higher Stefan numbers. The enthalpy solution has a significant difference for $St = 0.01$, which diminishes as St increases. This discrepancy can be attributed to how the enthalpy method defines the interface. In the presence of a mushy zone - a mixture of liquid and solid – the interface is considered to be the midpoint between the left and right boundaries of the mushy zone. In contrast, the sharp interface approach traces the point where the first transition from liquid to solid occurs, corresponding to the left end of the mushy zone. As shown in Fig. 7, where the mushy zone is plotted, the mushy zone is the largest for $St = 0.01$ and decreases as St increases.

In Fig. 4, we show temperature profiles during melting using the series solution with $St = 0.01, 0.1, 1$ and 10 . As can be seen especially in the case with $St = 0.01$, the temperature in the solid phase exceeds the melting temperature, creating an overheated region. Over time, this overheated region diminishes and eventually disappears. As the Stefan number increases, the overheating phenomenon persists but the duration and extent of the overheated zone decrease. This trend is also evident in Fig. 7 on the left, where we plot the evolution of the overheated zone using the series solution. It is clear that the width of the overheated zone rapidly increases from $\tau = 0$ until it reaches a maximum, and then it decays to zero. With $St = 0.01$, the initial growth rate is the fastest, the overheated zone peaks at $\tau = 0.4$, and then it starts to decay. As St increases, the initial growth rate decreases, the maximum width of the overheated zone also decreases, the overheated zone lasts for a shorter interval of time, and the overall overheating of the solid region reduces. This explains why the enthalpy solution has an almost constant difference from the series and front catching solutions at $St = 0.01$ but is closer to these solutions at higher Stefan numbers. During both melting and solidification, the interface approaches its steady state $\zeta \approx 0.45$ as time progresses using all methods. This is in agreement with

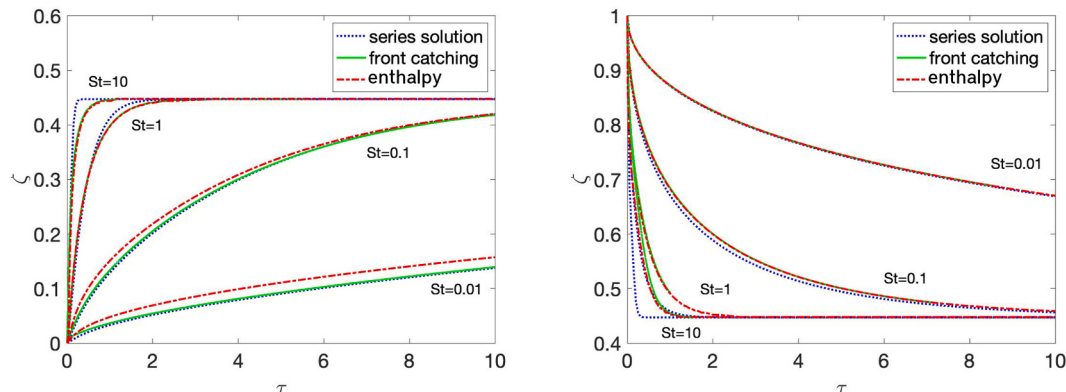


Fig. 3. Evolution of the front using the series solution, the method of catching the front into a space grid node and the enthalpy method for both melting (left) and solidification (right) with $\dot{Q} = 5$ and various values of the Stefan number. The enthalpy solutions are considered as reference solutions.

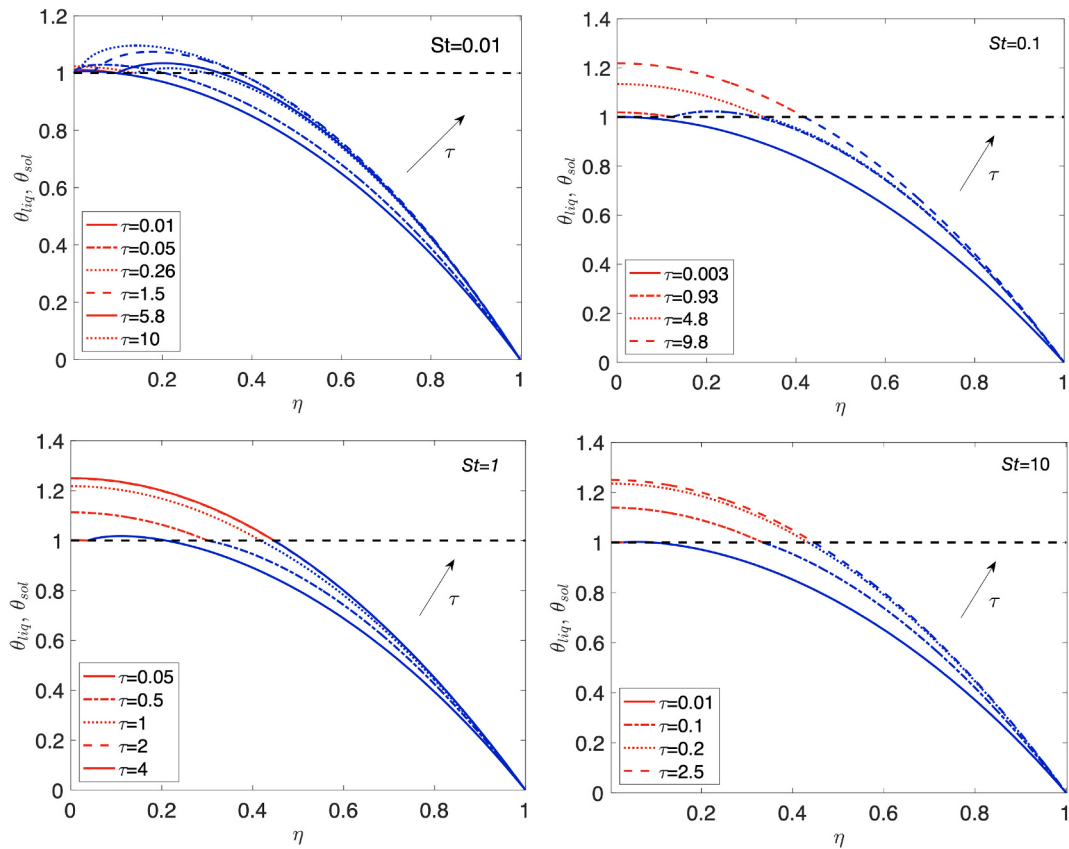


Fig. 4. Evolution of temperature during melting with $St = 0.01, 0.1, 1$ and 10 using the series solution. Red curves represent temperature in the liquid zone, blue curves - in the solid region. The black dashed parallel line at $\theta = 1$ corresponding to the dimensionless melting temperature. (For interpretation of the references to colour in this figure legend, the reader is referred to the web version of this article.)

the steady-state discussion in Section 4.1. The temperature evolution during melting using the front catching solution is illustrated in Fig. 5. Like the series solution, we observe overheating, although the extent of overheating is slightly reduced compared to the series solution. The temperature profiles obtained from the enthalpy method for the same values of St are depicted in Fig. 6. Notably, these solutions do not exhibit overheating. At later times, temperature profiles for all three methods are similar. Both the series solution method and the catching of the front into a node method are based on the sharp interface approach, i.e. no mushy zone is included in the model. The series solution method starts from considering the partial differential equations such as the heat equation and the interface energy equation but then after the solution splitting and separation of variables are implemented, the nonlinear ordinary differential equation for the interface is derived and solved numerically. The catching of the front into a node method solves the underlying partial differential equations, the heat equation and the interface energy equation, directly. In contrast to the series solution method and the catching of the front into a node method, the enthalpy method does not produce overheating. The fact that solutions to both series and front catching methods exhibit overheating in the solid phase indicates that the reason for overheating is the sharp interface modeling. The separation of variables step in obtaining series solutions may affect the solution behavior at earlier times but does not seem to be the reason for overheating.

In Fig. 7, we examine the evolution of the overheated zone using the series solution (left panel) and the mushy zone using the enthalpy solution (right panel). Both zones begin to develop early on. While the mushy zone reaches its maximum value and maintains about that same value for some time before rapidly decreasing to a small value, the overheated zone gradually diminishes after peaking. The decay is slower for $St = 0.01$ and faster for $St = 10$ in the overheated zone. The mushy

zone from the enthalpy solution persists longest for $St = 0.01$ and diminishes almost immediately for $St = 10$. Although the sharp interface approach does not explicitly model the mushy zone, the presence of the overheated zone suggests its existence. The shapes and durations of the overheated and mushy zones are similar to each other but the overheated zone decays more gradually than the mushy zone.

Temperature profiles during the solidification with $St = 1$, obtained using the series, front catching, and enthalpy methods, are illustrated in Fig. 8. The plots reveal remarkable similarity across all three methods. Notably, there is no overheating observed in either series or front catching solutions. Similar agreement is observed for other Stefan numbers among all three methods.

8.2. Prescribed heat flux case

Recall from the discussion of the quasi-static solution in Section 4.2 that $\frac{d\zeta}{dt} > 0$ when $Q'' < \frac{\dot{Q}}{2}$, indicating the interface ζ moves to the right, corresponding to melting. Conversely, $\frac{d\zeta}{dt} < 0$ occurs when $Q'' > \frac{\dot{Q}}{2}$, causing the interface to move to the left, indicating solidification. Therefore, to investigate melting, we choose $Q'' = 1.5, 2.0$ and 2.4 . For solidification, we set $Q'' = 2.6, 3.0$ and 4.0 . The internal heat generation remains fixed at $\dot{Q} = 5$.

The evolution of the interface during melting and solidification is illustrated in Fig. 9. During melting, depicted on the left, there is strong agreement between the enthalpy and front catching solutions. A zoom-in of the graphs shown in Fig. 10 superimposes an overheated region. Notably, for $Q'' = 1.5$, melting occurs most rapidly. The enthalpy and front catching solutions have a small discrepancy during the presence of the overheated zone. Otherwise they show excellent agreement. The quasi-static solution moves fastest among all methods, whereas the

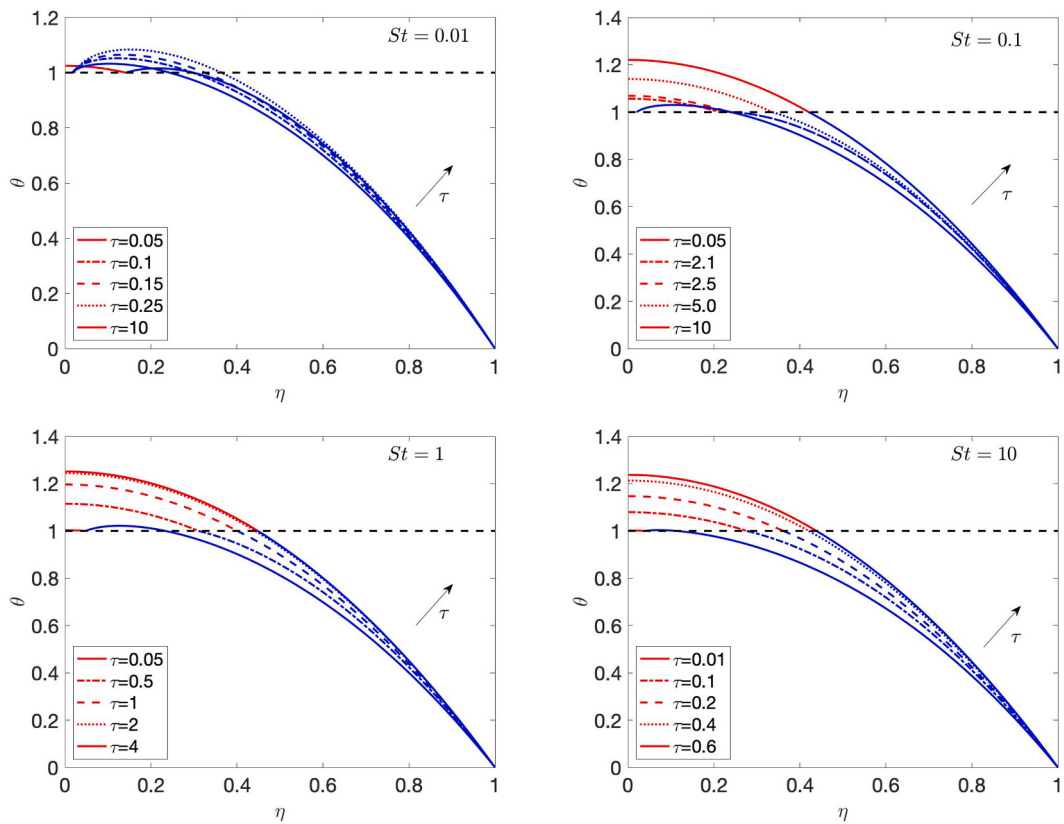


Fig. 5. Evolution of temperature during melting with $St = 0.01$ (left) and $St = 0.1$ (right) using the front catching method.

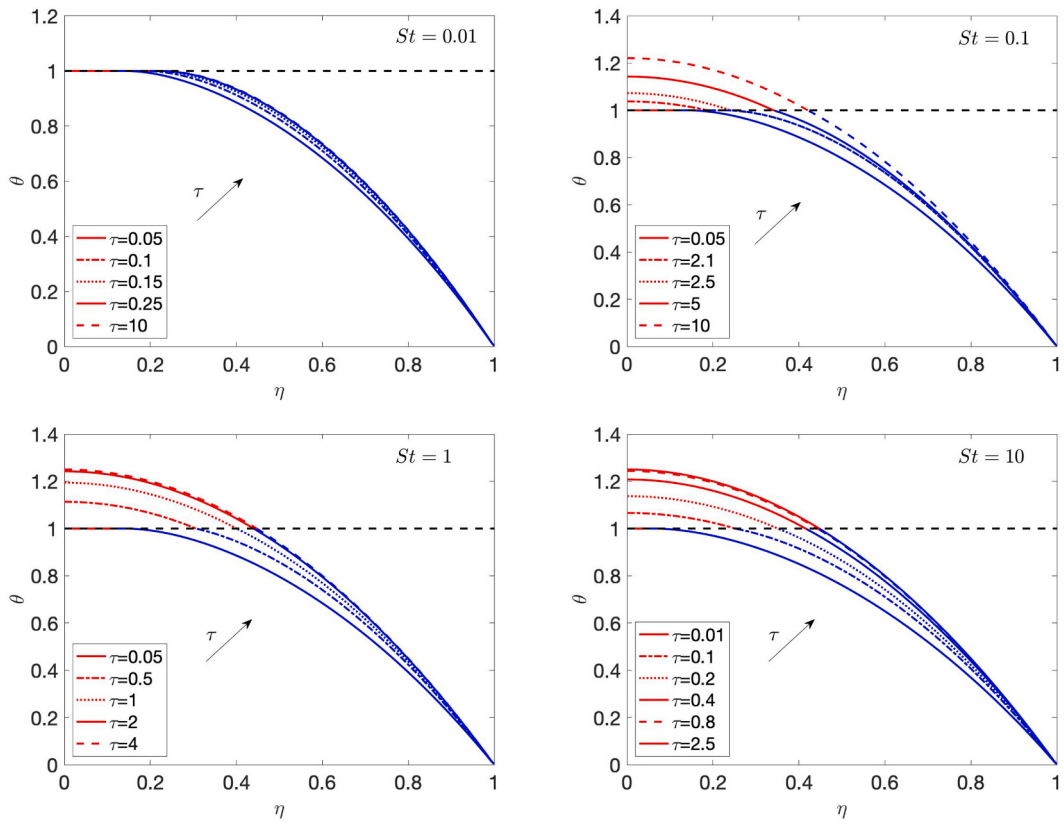


Fig. 6. Evolution of temperature during melting with $St = 0.01$ (left) and $St = 0.1$ (right) using the enthalpy method.

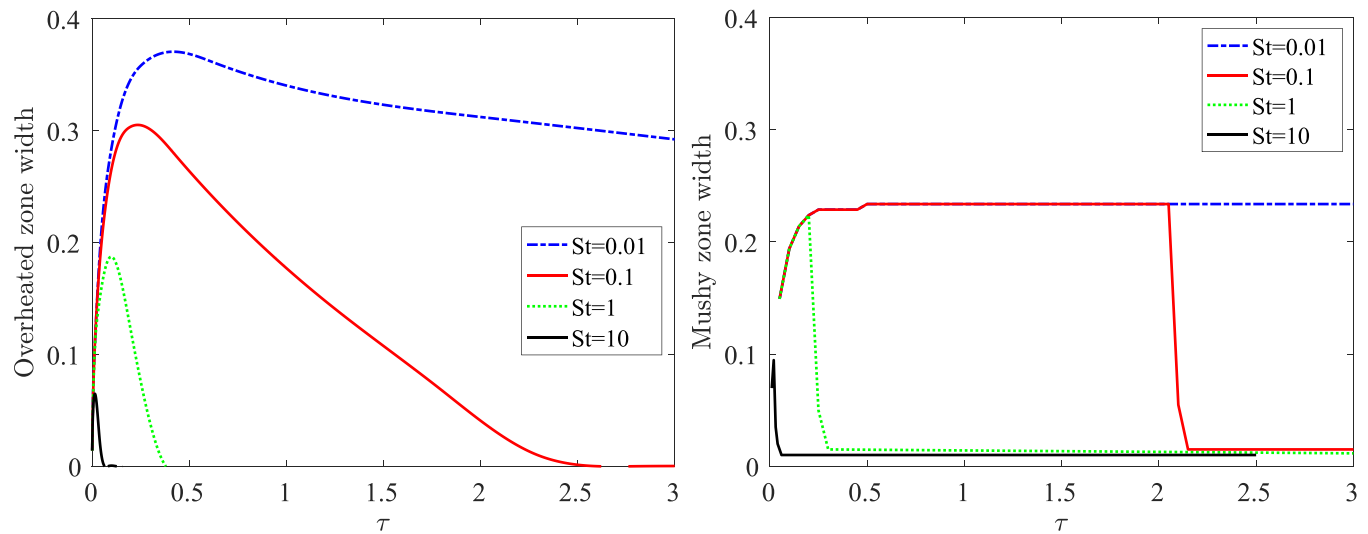


Fig. 7. Evolution of the overheated zone (left) generated by using the series solution compared to the evolution of the mushy zone (right) obtained by using Ansys Fluent software for the case of the prescribed constant temperature at the boundary of the cylinder.

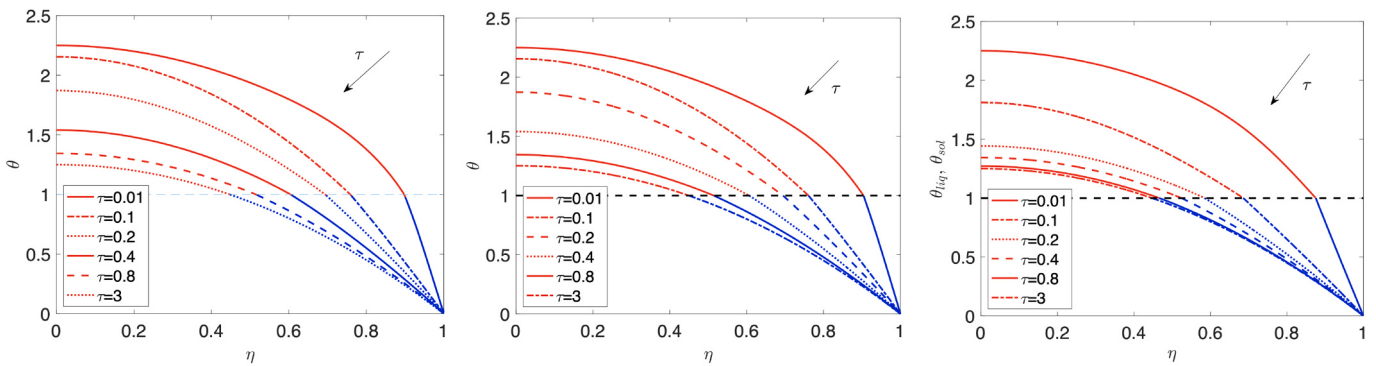


Fig. 8. Evolution of temperature during solidification with $St = 1$ using the series solutions (left), front catching solutions (middle) and using the enthalpy method (right).

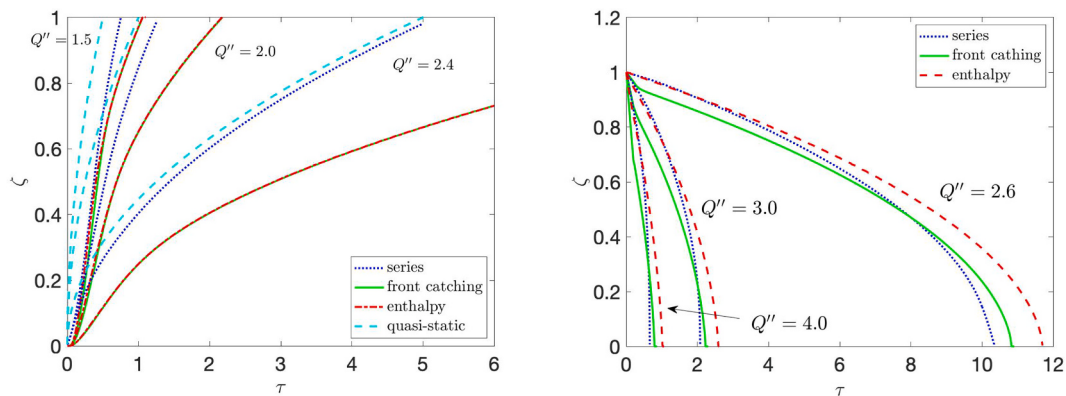


Fig. 9. Evolution of the interface using the series (blue dotted), front catching (green solid), enthalpy (red dash dotted), quasi-static (cyan dashed) during melting (left panel) and solidification (right panel). (For interpretation of the references to colour in this figure legend, the reader is referred to the web version of this article.)

series solution is in-between. Initially, the series solution closely tracks the enthalpy solution for early times but gradually diverges, reaching the outer boundary sooner. For $Q'' = 2.0$, melting slows down, resulting in a smaller and shorter overheated zone. As a result, the enthalpy and front catching solutions exhibit better agreement than in the case with $Q'' = 1.5$, although discrepancies arise during the overheated/mushy zone. The series solution remains faster than the enthalpy solution,

especially at later times, but the discrepancy is smaller than with the quasi-static solution. The case with $Q'' = 2.4$ corresponds to the slowest melting considered here. This is because the amount of heat generated inside the material is just a little bit higher than the amount of heat taken out at the outer boundary. The enthalpy and front catching solutions are almost indistinguishable, which is in agreement with a very small and short overheated/mushy zone. Both series and quasi-static solutions

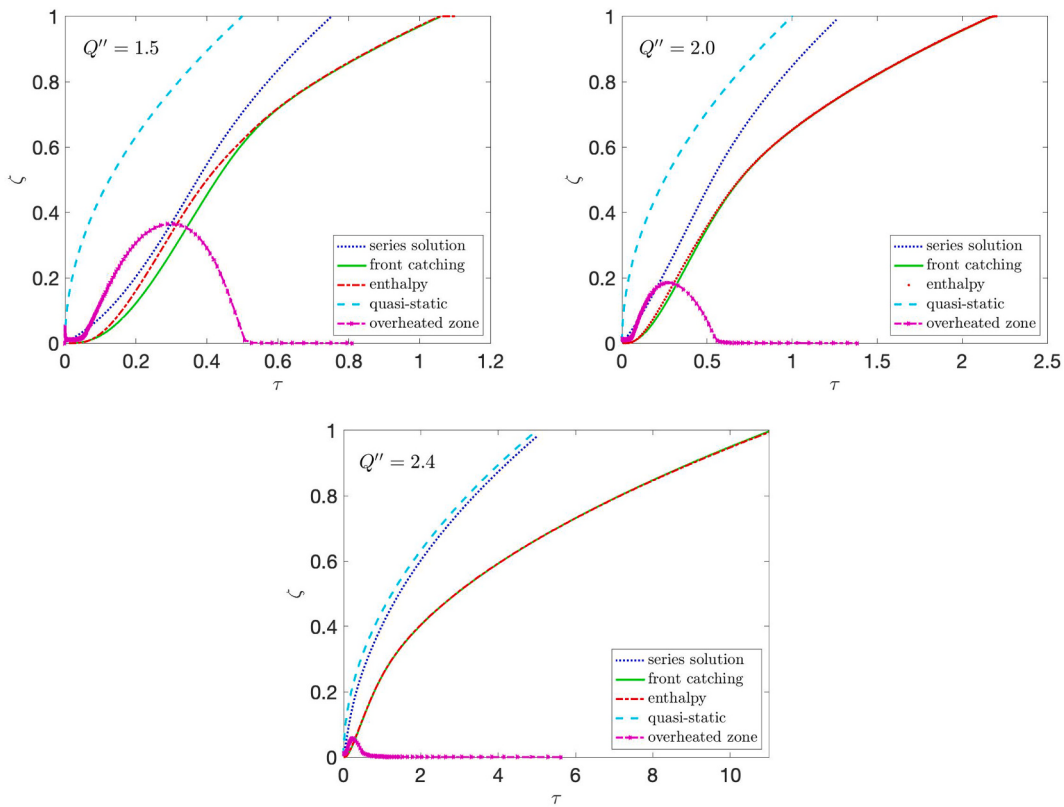


Fig. 10. Zoom-in: evolution of the interface using the series (blue dotted), front catching (green solid), enthalpy (red dash dotted), quasi-static (cyan dashed), for $Q'' = 1.5, 2.0$, and 2.4 in the case of the prescribed constant heat flux at the boundary of the cylinder. At the end of each simulation time, the material is completely melted. Superimposed is the evolution of the corresponding overheated zone. (For interpretation of the references to colour in this figure legend, the reader is referred to the web version of this article.)

outpace enthalpy and front catching solutions, with the series solution closer to enthalpy, despite some deviation. The slow melting rate allows more time for interface to deviate from the enthalpy and front catching solutions compared to faster melting rates. The evolution of the interface during the solidification, shown on the right of Fig. 9, indicates similar profiles across all methods. The series solution agrees well with the enthalpy solutions initially but reaches the centerline slightly earlier. The solidification in front catching solutions initially is faster than with other methods but then it slows down. Front catching solutions reach the centerline later than series solutions but sooner than the enthalpy solutions. Overall, it is notable that there is more agreement between all solutions for $Q'' = 4.0$, reflecting faster front movement similar to the melting scenario, since it takes much less time for the solutions to reach the centerline.

The evolution of temperature during melting for series, front catching, and enthalpy methods is depicted in Figs. 11, 12 and 13, respectively. Both the series and front catching solutions show overheating, particularly noticeable for Q'' around to $Q''/2 = 2.5$. In contrast, the enthalpy solutions do not exhibit this overheating phenomenon.

In Fig. 14, we compare the evolution of the overheated zone using the front catching solution with the mushy zone from the enthalpy method. The overheated zone obtained with the series solution is similar to that of the front catching solution. Across all three case of Q'' considered, the shapes and duration of the zones are very similar. The largest mushy/overheated zones occur with $Q'' = 1.5$, while the smallest and shortest zones are observed with $Q'' = 2.4$.

The temperature profiles during solidification with $Q'' = 3$ for the series and enthalpy methods are shown in Fig. 15. Both methods exhibit

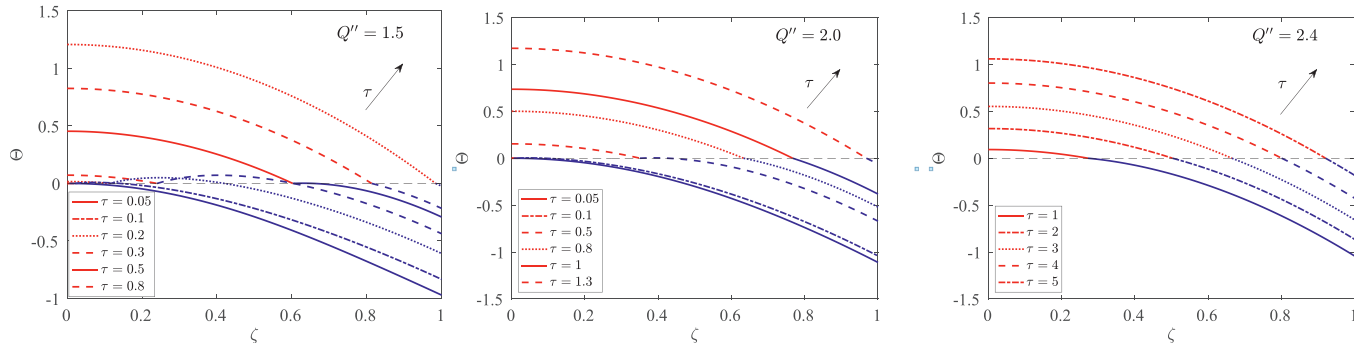


Fig. 11. Evolution of the temperature for $Q'' = 1.5$ (left panel), $Q'' = 2.0$ (middle panel) and $Q'' = 2.4$ (right panel) using the series solution. The temperature profiles in the solid phase for $Q'' = 1.5$ show the overheating phenomenon where the temperature in the solid exceed the dimensionless melting temperature $\Theta = 0$ represented by the black dashed line.

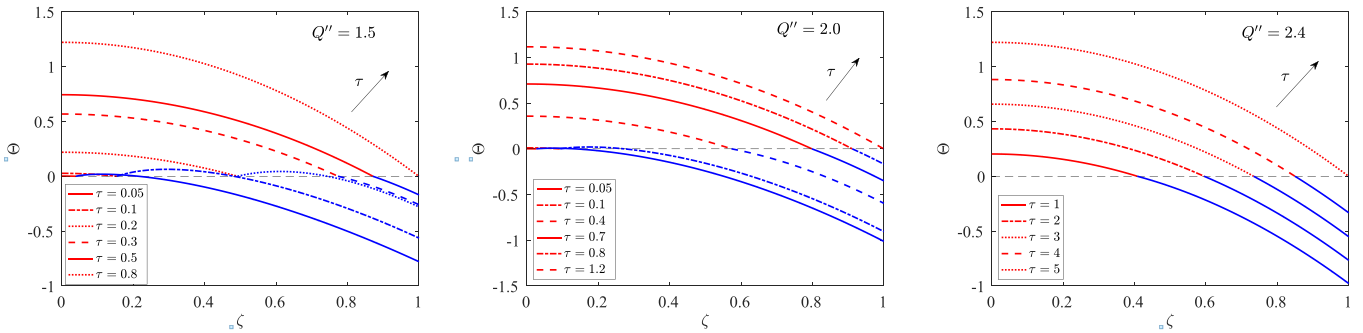


Fig. 12. Evolution of the temperature for $Q'' = 1.5$ (left panel), $Q'' = 2.0$ (middle panel) and $Q'' = 2.4$ (right panel) using the front catching solution. The temperature profiles in the solid phase for $Q'' = 1.5$ show the overheating phenomenon where the temperature in the solid exceed the dimensionless melting temperature $\Theta = 0$.

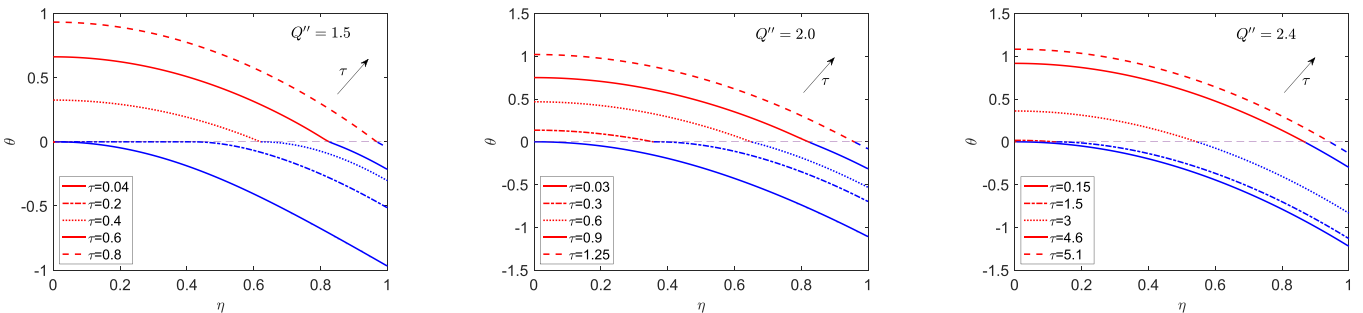


Fig. 13. Evolution of the temperature for $Q'' = 1.5$ (left panel), $Q'' = 2.0$ (middle panel) and $Q'' = 2.4$ (right panel) using the enthalpy method. No overheating phenomenon is observed.

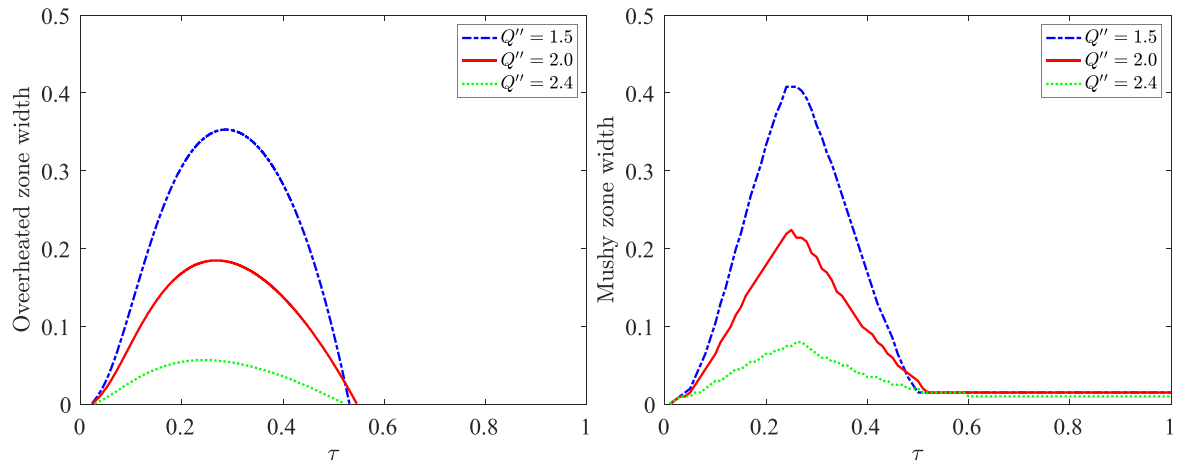


Fig. 14. Evolution of the overheated zone (left) generated by using the front catching solution compared to the evolution of the mushy zone (right) obtained by using Ansys Fluent software for the case of the prescribed constant flux at the boundary of the cylinder.

very similar results. The profiles for the front catching solution, not shown here, also agree well with the series and enthalpy methods.

9. Conclusions

We explore the problem of solid-liquid phase change with internal heat generation, considering two cases: (1) prescribed constant temperature and (2) heat flux at the outer boundary of an infinite cylinder. This scenario extends the classical Stefan problem by incorporating internal heat sources like radioactive decay. The phase transition between liquid and solid phases is modeled using a sharp interface approach. We assume that the interface moves slowly compared to temperature changes in both phases. This weakly time-dependent assumption

enables us to split the solution in each phase into transient and quasi steady-state solutions. The transient part is solved by the method of separation of variables, while the quasi steady-state solution is obtained through direct integration. We derive a nonlinear first-order ordinary differential equation for the interface, that includes infinite Fourier-Bessel series terms, which can be solved numerically using standard ODE methods. Additionally, we compare this semi-analytical approach with the catching of the front into a space grid node method as well as the enthalpy-porosity method, which accounts for a mushy zone or a mixed solid-liquid region.

During melting with a prescribed constant outer temperature, we observe excellent agreement between the series and front catching solutions, especially for small Stefan numbers. Discrepancies with

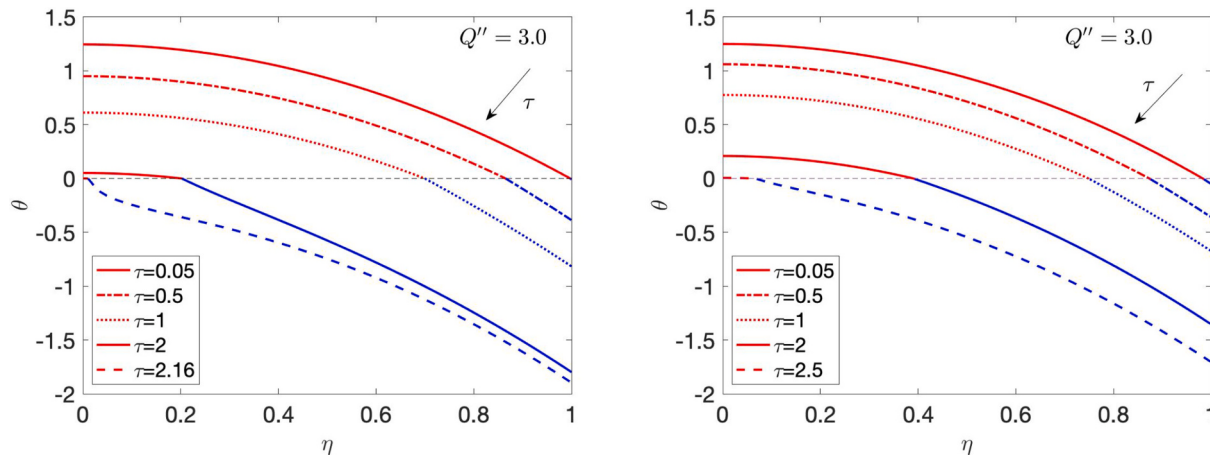


Fig. 15. Evolution of the temperature during the solidification process for $Q'' = 3.0$ using the series (left) and enthalpy (right) methods.

enthalpy solutions at low Stefan numbers arise due to the presence of the mushy zone and how the interface is defined by the enthalpy method. These differences diminish as the mushy zone shrinks. At higher Stefan numbers, the series solutions reach steady-state slightly faster than the front catching and enthalpy solutions. Both series and front catching temperature solutions exhibit an overheating phenomenon since the sharp interface model does not allow a mushy zone. We find that the overheated and mushy zones have a similar evolution.

For prescribed heat flux at the outer boundary, the front catching and enthalpy solutions during melting align very well except during times when a mushy zone is large in both temperature and duration. Series solutions reach the outer boundary slightly earlier than front catching and enthalpy solutions, though they remain closer to enthalpy and front catching solutions than the quasi-static solutions. In both problems, the general trends in the solutions during solidification agree between all the methods. Although the sharp-interface approach does not assume the existence of a mushy zone, it produces an overheated region in the solid phase during the melting process, that resembles a mushy zone.

We hope that the present paper will stimulate experimental research, particularly on phase change in materials with internal heat generation to validate and extend theoretical and numerical findings.

CRediT authorship contribution statement

Lyudmyla L. Barannyk: Writing – review & editing, Writing – original draft, Visualization, Validation, Methodology, Investigation, Formal analysis, Data curation, Conceptualization. **John C. Crepeau:** Writing – review & editing, Writing – original draft, Project administration, Methodology, Investigation, Conceptualization. **Patrick Paulus:** Visualization, Validation, Methodology, Investigation, Data curation. **Alexey Yu. Sakhnov:** Writing – review & editing, Writing – original draft, Visualization, Validation, Methodology, Investigation, Formal analysis, Data curation, Conceptualization. **Sidney D.V. Williams:** Writing – review & editing, Writing – original draft, Visualization, Validation, Methodology, Investigation, Formal analysis, Data curation.

Declaration of competing interest

The authors declare that they have no known competing financial interests or personal relationships that could have appeared to influence the work reported in this paper.

Data availability

Data will be made available on request.

References

- [1] G. Lamé, B. Clapeyron, Mémoire sur la solidification par refroidissement d'un globe liquide, Ann. Chim. Phys. 47 (1831) 250–256.
- [2] J. Stefan, Ueber die theorie der eisbildung, insbesondere über die eisbildung im polarmeere, Sitzungsberichte der k.k. Akademie der Wissenschaften, Abteilung II (1889) 965–983.
- [3] L. Rubenstein, The Stefan Problem, AMS Pubs, Providence, 1971.
- [4] V. Alexiades, A. Solomon, Mathematical Modeling of Melting and Freezing Processes, Hemisphere, 1993.
- [5] G. Lock, Latent Heat Transfer, Oxford, 1994.
- [6] N. Salva, D. Tarzia, Explicit solutions for a Stefan problem with variable latent heat and constant heat flux boundary conditions, J. Math. Anal. Appl. 379 (2011) 240–244.
- [7] J. Crepeau, A. Siahpush, Approximate solutions to the Stefan problem with internal heat generation, Heat Mass Transf. 44 (2008) 787–794.
- [8] Z.T. Yu, L.W. Fan, Y.C. Hu, K.F. Cen, Perturbation solutions to heat conduction in melting or solidification with heat generation, Heat Mass Transf. 46 (2010) 479–483.
- [9] C. An, J. Su, Lumped parameter model for one-dimensional melting in a slab with volumetric heat generation, Appl. Therm. Eng. 60 (2013) 387–396.
- [10] Rai K.N. Jitendra, J. Singh, A numerical study on non-fourier heat conduction model of phase change problem with variable internal heat generation, J. Eng. Math. 129 (2021).
- [11] S. Weinstein, Catastrophic overturn of the Earth's mantle driven by multiple phase changes and internal heat generation, Geophys. Res. Lett. 20 (1993) 101–104.
- [12] K. Furlong, D. Chapman, Heat flow, heat generation, and the thermal state of the lithosphere, Annu. Rev. Earth Planet. Sci. 41 (2013) 385–410.
- [13] Z.H. Rao, S.F. Wang, Y.L. Zhang, Simulation of heat dissipation with phase change material for cylindrical power battery, J. Energy Inst. 85 (2012) 38–43.
- [14] W.B. Ye, M. Arici, Numerical thermal control design for applicability to a large-scale high-capacity lithium-ion energy storage system subjected to forced cooling, Numer. Heat Transf. Part A Appl. 0 (2024) 1–15.
- [15] M. Bechiri, K. Mansouri, Analytical study of heat generation effects on melting and solidification of nano-enhanced PCM inside a horizontal cylindrical enclosure, Appl. Therm. Eng. 104 (2016) 779–790.
- [16] M. Barzegari, M. Aghaie, A. Zolfaghari, Assessment of fuel-rod meltdown in a severe accident at Bushehr nuclear power plant (bnpp), Nucl. Sci. Tech. 30 (2019).
- [17] W. Chen, M. Ishii, M. Grolmes, Simple heat conduction model with phase change for reactor fuel pin, Nucl. Sci. Eng. 60 (1976) 452–460.
- [18] M. El-Genk, A. Cronenberg, An assessment of fuel freezing and drainage phenomena in a reactor shield plug following a core disruptive accident, Nucl. Eng. Des. 47 (1978) 195–225.
- [19] F. Cheung, T. Chawla, D. Pedersen, The effects of heat generation and wall interaction on freezing and melting in a finite slab, Int. J. Heat Mass Transf. 27 (1984) 29–37.
- [20] S. Chan, D. Cho, G. Kocamustafaogullari, Melting and solidification with internal radiative transfer—a generalized phase change model, Int. J. Heat Mass Transf. 26 (1983) 621–633.
- [21] S. Chan, K. Hsu, Applications of a generalized phase change model for melting and solidification of materials with internal heat generation, in: Proceedings of the AIAA 19th Thermophysics Conference, Snowmass, CO, 1984.
- [22] R. Le Tellier, E. Skrzypek, L. Saas, On the treatment of plane fusion front in lumped parameter thermal models with convection, Appl. Therm. Eng. 120 (2017) 314–326.
- [23] J. Tang, M. Huang, Y. Zhao, S. Maqsood, X. Ouyang, Numerical investigations on the melting process of the nuclear fuel rod in RIAs and LOCA, Int. J. Heat Mass Transf. 124 (2018) 990–1002.
- [24] A. Dubey, A. Sharma, Melting and multi-phase flow modelling of nuclear fuel in fast reactor fuel rod, Int. J. Therm. Sci. 125 (2018) 256–272.

- [25] C. An, F. Moreira, J. Su, Thermal analysis of the melting process in a nuclear fuel rod, *Appl. Therm. Eng.* 68 (2014) 133–143.
- [26] R.A. Alsulami, T.M. Zope, K. Premnath, M. Aljaghtham, Convectively cooled solidification in phase change materials in different configurations subject to internal heat generation: quasi-steady analysis, *Appl. Therm. Engr.* 221 (2023) 119849.
- [27] Z. Wang, Z. Han, Z. Liang, W. Deng, Z. Xu, Modeling of the frost layer's growth considering its melting and re-solidification, *Int. J. Heat Mass Transf.* 218 (2024) 124777.
- [28] W.B. Ye, M. Arici, 3d validation, 2d feasibility, corrected and developed correlations for pure solid-gallium phase change modeling by enthalpy-porosity methodology, *Int. Commun. Heat Mass Transf.* 144 (2023).
- [29] W.B. Ye, M. Arici, False diffusion, asymmetric interface, and equilibrious state for pure solid-gallium phase change modeling by enthalpy-porosity methodology, *Int. Commun. Heat Mass Transf.* 144 (2023).
- [30] W.B. Ye, M. Arici, Redefined interface error, 2d verification and validation for pure solid-gallium phase change modeling by enthalpy-porosity methodology, *Int. Commun. Heat Mass Transf.* 147 (2023).
- [31] W.B. Ye, M. Arici, Exploring mushy zone constant in enthalpy-porosity methodology for accurate modeling convection-diffusion solid-liquid phase change of calcium chloride hexahydrate, *Int. Commun. Heat Mass Transf.* 152 (2024).
- [32] L. Barannyk, J. Crepeau, P. Paulus, A. Siahpush, Fourier-Bessel series model for the Stefan problem with internal heat generation in cylindrical coordinates, in: 26th International Conference on Nuclear Engineering ICONE26, July 22–26, London, England, 2018 pp. ICONE26–81009.
- [33] D. McCord, J. Crepeau, A. Siahpush, J. Ferris Brogin, Analytical solutions to the Stefan problem with internal heat generation, *Appl. Therm. Eng.* 103 (2016) 443–451.
- [34] S. Williams, L. Barannyk, J. Crepeau, P. Paulus, The Stefan problem with internal heat generation in spherical coordinates, *J. Heat Transf.* 144 (2022) 092401.
- [35] J.C. Crepeau, A.Y. Sakhnov, V.S. Naumkin, Stefan problem with internal heat generation: comparison of numerical modeling and analytical solution, *J. Phys. Conf. Ser.* 1369 (2019) 012025.
- [36] L.L. Barannyk, S.V. Williams, J.C. Crepeau, O.I. Ogida, A. Sakhnov, On the Stefan Problem with Internal Heat Generation and Prescribed Heat Flux Conditions at the Boundary, in: Proceedings of the ASME 2019 Summer Heat Transfer Conference HT2019 July 15–18, 2019, Bellevue, WA, USA, 2019 pp. HT2019–3703.
- [37] J. Crepeau, A. Siahpush, B. Spotten, On the Stefan problem with volumetric energy generation, *Heat Mass Transf.* 46 (2009) 119–128.
- [38] P. Paulus, Analytical and Numerical Modeling of Solid-Liquid Phase Change Driven by Internal Heat Generation in Cylindrical Coordinates, Master's thesis, University of Idaho, Moscow, ID 83844, USA, 2021, 875 Perimeter Dr.
- [39] V. Voller, C. Prakash, A fixed grid numerical modelling methodology for convection-diffusion mushy region phase-change problems, *Int. J. Heat Mass Transf.* 30 (1987) 1709–1719.
- [40] ANSYS, Inc, ANSYS FLUENT 12.0 Theory Guide. <https://www.ansys.com/doc/12.0/fluent/theory/>, 2009.
- [41] M. Worster, The dynamics of mushy layers, in: *Interactive Dynamics of Convection and Solidification* vol. 219, Springer, 1992, p. 289.
- [42] F. Incropiera, D. DeWitt, *Introduction to Heat Transfer*, Wiley, New York, 2002.
- [43] D. Poulikakos, *Conduction Heat Transfer*, Prentice-Hall, Englewood Cliffs, 1994.
- [44] A. Shrivastava, B. Williams, A. Siahpush, B. Savage, J. Crepeau, Numerical and experimental investigation of melting with internal heat generation within cylindrical enclosures, *Appl. Therm. Eng.* 68 (2014) 587–596.
- [45] A.A. Samarskii, P.N. Vabishchevich, Computational heat transfer, in: *Volume 1 of Mathematical Modelling*, John Wiley & Sons Ltd., 1995.
- [46] R. Haberman, *Applied Partial Differential Equations with Fourier Series and Boundary Value Problems*, Volume 5th Edition of Pearson Modern Classics for Advanced Mathematics Series, Pearson, 2018.
- [47] E. Kreyszig, *Advanced Engineering Mathematics*, 9th ed., Wiley, New York, 2005.
- [48] T.J. Dekker, Finding a Zero by Means of Successive Linear Interpolation, in: *Constructive Aspects of the Fundamental Theorem of Algebra*, Interscience, 1969, p. 337.
- [49] T.J. Dekker, W. Hoffmann, *Algol 60 Procedures in Numerical Algebra. Volume Parts 1 and 2, Tracts 22 and 23*, Mathematisch Centrum Amsterdam, 1968.
- [50] C. Moler, Zeroin, part 1: Dekker's algorithm, URL, <https://blogs.mathworks.com/cleve/2015/10/12/zeroin-part-1-dekkers-algorithm/>, 2015.
- [51] L.F. Shampine, M.W. Reichelt, The MATLAB ODE suite, *SIAM J. Scie. Comp.* 18 (1997) 1–22.
- [52] W. Elenbaas, Heat dissipation of parallel plates by free convection, *Physica* 9 (1942) 2–28.
- [53] V. Terekhov, A. Ekaid, Laminar natural convection between vertical isothermal heated plates with different temperatures, *J. Engr. Thermophys.* 20 (2011) 416–433.
- [54] V. Terekhov, A. Ekaid, K. Yassin, Laminar free convection heat transfer between vertical isothermal plates, *J. Engr. Thermophys.* 25 (2016) 509–519.
- [55] V.M. Zheleznyak, A.K. Panjushkin, A.I. Sharikov, E.G. Bek, A.S. Doronin, A. S. Duhovenskij, J.K. Bibilashvili, V.A. Mezhuev, P.I. Lavrenjuk, V.V. Rozhkov, A. A. Enin, M.V. Popozov, A.I. Kushmanov, Abstract of Invention RU 2244347 C2: Fuel Rod for Water-Moderated Water-Cooled Power Reactor, Russian Federation Federal Service for Intellectual Property, Patents and Trademarks, 2005 (in Russian).
- [56] S. Andrushechko, A. Afrov, B. Vasilev, V. Generalov, K. Kosourov, Y. Semchenkov, V. Ukraintsev, Nuclear Power Plant with Reactor WWER-1000. Logos (in Russian), Moscow, 2010.
- [57] P. Kirillov, G. Bogoslovskaya, *Heat Transfer in Nuclear Power Stations*. Energoatomizdat (in Russian), Moscow, 2000.
- [58] A.D. Anderson, J.C. Tannehill, R.H. Pletcher, *Computational Fluid Mechanics and Heat Transfer*, Hemisphere, London, 1985.
- [59] R. Pletcher, J. Tannehill, D. Anderson, *Computational Fluid Mechanics and Heat Transfer*, CRC Press, Boca Raton, Florida, 2012.
- [60] V.R. Voller, Fast implicit finite-difference method for the analysis of phase change problems, *Numer. Heat Transf. B Fundam.* 17 (1990) 155–169.